Reconstruction of the Advanced Supersonic Parachute Inflation Research Experiment Sounding Rocket Flight Test

Christopher D. Karlgaard*and Jake A. Tynis†
Analytical Mechanics Associates, Inc., Hampton, VA

Clara O'Farrell‡
Jet Propulsion Laboratory, California Institute of Technology, Pasadena, CA

The Advanced Supersonic Parachute Inflation Research and Experiments project is a flight test program for development of supersonic parachutes for potential future use at Mars. The flight tests are designed to reduce risk for the Mars 2020 mission. The flight tests involve two Disk-Gap-Band parachute designs to be tested at relevant Mach number and dynamic pressure conditions for the Mars 2020 entry capsule. The first of these parachutes is a built-to-print design that was successfully employed by the Mars Science Laboratory lander at Mars in August 2012, and the second is a design that is strengthened in material properties and construction methods but has the same geometry as that used by Mars Science Laboratory. The first flight test of the built-to-print parachute took place on October 4, 2017 at NASA's Wallops Flight Facility. This paper describes the instrumentation, data analysis techniques, and atmospheric and trajectory reconstruction results from this flight test.

I. Introduction

The Advanced Supersonic Parachute Inflation Research and Experiments (ASPIRE) project[1] is a risk reduction[2] flight test program for testing the Mars 2020 parachute system. The ASPIRE project uses sounding rocket flights to deploy parachutes at high altitude on Earth to simulate Mars-relevant deployment conditions. Two Disk-Gap-Band (DGB)[3] parachute designs are being evaluated by the ASPIRE project. The first of these is a built-to-print version of the DGB that was successfully deployed at Mars during the Mars Science Laboratory (MSL) mission in August 2012. The second parachute is a strengthened version that has the same geometry but uses improved materials and construction methods.

The ASPIRE projects tests these parachutes using Terrier-Black Brant sounding rockets to launch a payload to high altitude on Earth to simulate the relevant deployment conditions at Mars. The sounding rockets are launched over the Atlantic ocean from NASA's Wallops Flight Facility (WFF). The payload consists of the parachute pack, the deployment mortar, and the ASPIRE instrumentation suite. The test vehicle configurations are shown in Figures 1 and 2. The ASPIRE concept of operations is shown in Figure 3.

The onboard instrumentation suite included an Inertial Measurement Unit (IMU), a Global Positioning System (GPS) unit, a C-band transponder for radar tracking, three load pins at the parachute triple bridles, and three high-speed/high-resolution cameras trained on the canopy during inflation. In addition, the atmospheric conditions at the time of flight were characterized by means of high-altitude meteorological balloons carrying radiosondes. These data allowed the reconstruction of the test conditions, parachute loads, and parachute aerodynamic performance in flight. In addition, the imagery from the on-board cameras will allow the reconstruction of the three-dimensional geometry of the canopy during inflation.

The first flight test (SR01) of the built-to-print DGB parachute took place on October 4, 2017. The test conditions for the first ASPIRE flight were chosen to replicate those seen by the MSL parachute at Mars in 2012. Reconstruction

*Supervising Engineer, Senior Member AIAA.
†Aerospace Engineer, Member AIAA.
‡Guidance and Control Engineer, Member AIAA.

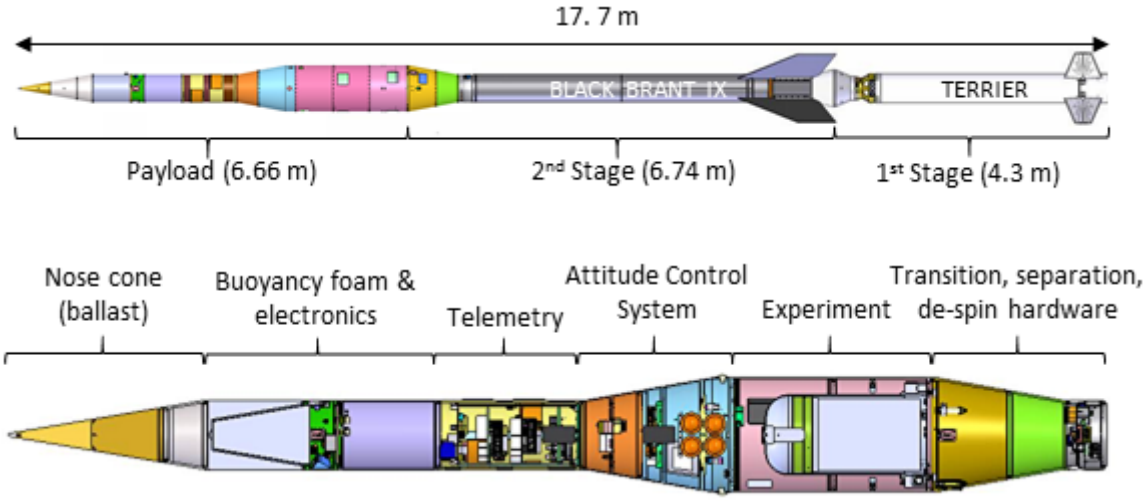

Figure 1: ASPIRE SR01 Launch and Payload Configuration

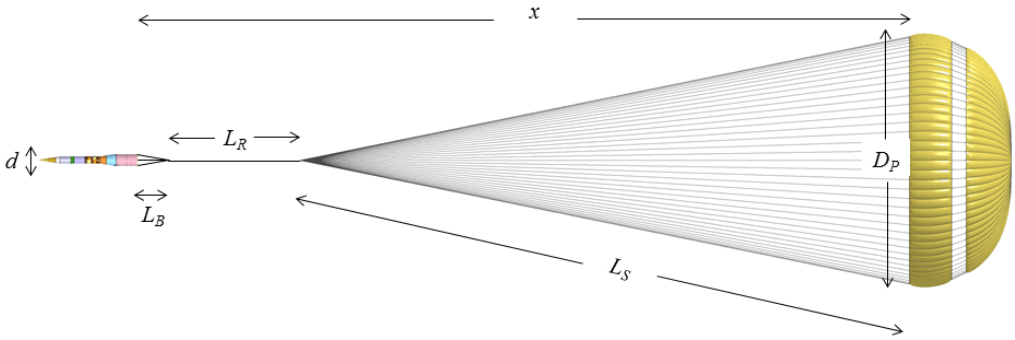

Figure 2: ASPIRE SR01 System Configuration

of the MSL parachute's performance after landing [4] estimated a Mach number of approximately 1.7 and a dynamic pressure of 474 Pa at the moment of peak load. This paper describes the SR01 flight test and provides an overview of flight operations, the data acquired during testing, the techniques used for post-flight reconstruction, and the reconstructed trajectory and as-flown atmosphere. Additional details on parachute reconstructed performance can be found in [5], and simulation reconciliation results can be found in [6].

II. Instrumentation and Measurements

A variety of measurement sources were available for use in the trajectory and atmosphere reconstruction process. These measurements included onboard instrumentation such as an IMU and GPS receiver; ground-based measurements from tracking radars; and atmospheric soundings from balloons. The following sections provide a more detailed overview of the measurement sources and their performance on the day of flight.

A. Inertial Measurement Unit

Three-axis linear accelerations and angular rates were measured by a Gimbaled LN-200 with Miniature Airborne Computer (GLN-MAC) inertial navigation system. The LN-200 inertial measurement unit contains three-axis solid-state silicon Micro Electro-Mechanical System (MEMS) accelerometers and three-axis solid state fiber-optic gyroscopes. The GLN-MAC incorporates a roll isolation gimbal to produce a stable platform for spinning vehicle applications. An electric motor is used to counter-rotate the internal mount plate such that the LN-200 senses a low rotational

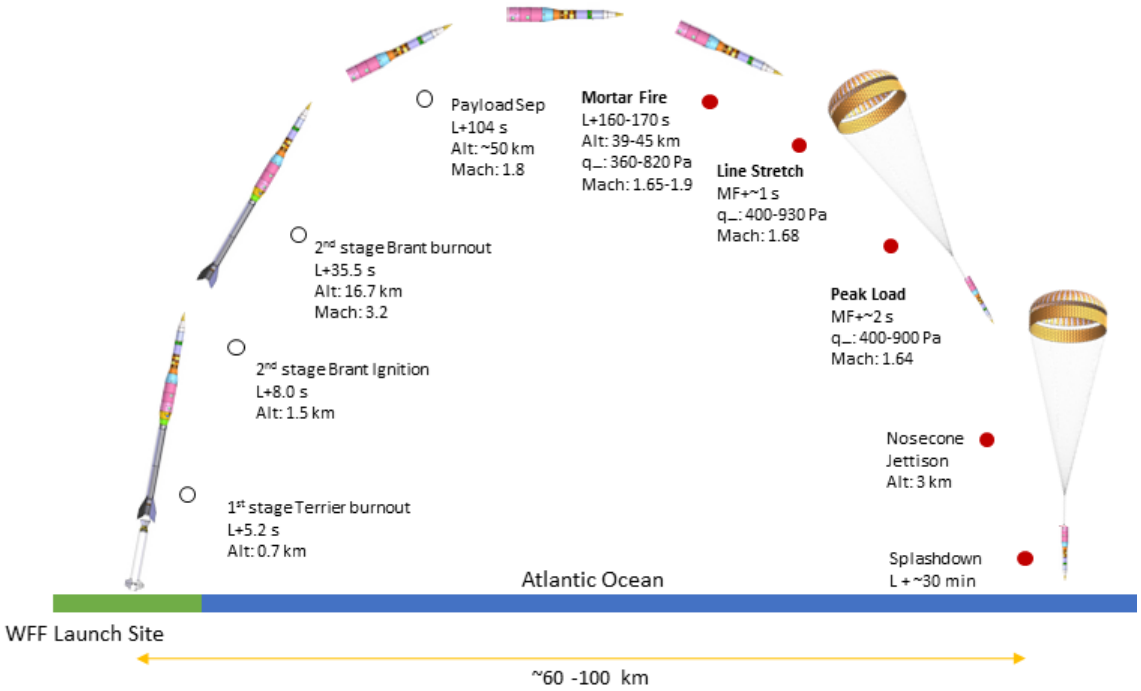

Figure 3: ASPIRE SR01 Concept of Operations

rate about the spin axis. The gimbaling has the effect of reducing error buildup due to scale factor uncertainties in the roll gyro. The angle of the mount plate is measured with a resolver. The GLN-MAC has the capability to cage or lock the LN-200 in a preferred orientation, creating a true strapdown IMU. This mode was not used for the SR01 flight; the LN-200 was free to gimbal throughout the entire flight test.

The GLN-MAC produces two sets of telemetry, one from the gimbaled LN-200 at a rate of 400 Hz and one from the integrated GLN-MAC system at a rate of 100 Hz. The resolver angle is also telemetered at a rate of 400 Hz. The GLN-MAC level outputs utilize the resolver angle and resolver rate to generate an equivalent strapdown representation of the gimbaled LN-200 accelerations and rates. Typical performance characteristics of the GLN-MAC sensor can be found in [7]. The raw LN-200 data was corrected post-flight for known thermal biases and misalignments prior to its use in the trajectory reconstruction. There were intermittent dropped frames from the GLN-MAC telemetry but these were isolated to single frames and thus did not degrade the reconstruction. The effective sample rate of the LN-200 data is shown in Figure 4.

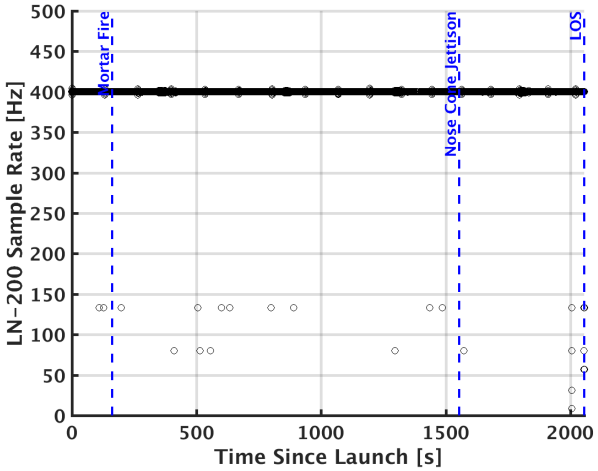

Figure 4: LN-200 Sample Rate

The GLN-MAC was a primary component of the NASA Sounding Rocket Operations Contract (NSROC) Inertial Attitude Control System (NIACS), which was located on the ACS section of the payload. The NIACS consists of the GLN-MAC and a set of cold-gas thrusters. A set of four cold-gas thrusters located at 90 deg intervals around the circumference of the experiment section is used to maintain a near-zero total angle of attack leading up to parachute deploy. Two pairs of roll-axis thrusters (a clockwise pair and a counter-clockwise pair) are used to null any residual roll rate following de-spin and separation from the second stage.

The NIACS was also responsible for triggering the firing of the parachute mortar at the desired dynamic pressure. During flight, the NIACS computes an on-board vehicle state from the IMU measurements and GPS-derived position and velocity. This navigation solution provides an estimate of the inertial velocity and altitude throughout the flight. Prior to launch, polynomial models for atmospheric winds, density, and temperature as a function of altitude were loaded onto the NIACS. These polynomials were then evaluated during flight to obtain an on board estimate of the wind-relative dynamic pressure which was used to trigger parachute deployment. Simulations of the payload's trajectory along with estimates of the time from mortar fire to peak load were used to derive a NIACS trigger value of 384 Pa. Once that dynamic pressure was calculated, the NIACS initiated a series of events, including turning off the ACS, starting the high speed camera recording, deploying the camera lens covers, and, 1.4 seconds after the dynamic pressure trigger is reached, signaling of the mortar to fire.

B. Global Positioning System

Measurements of position and velocity were obtained from a Javad TR-G2 HDA GPS receiver at a rate of 20 Hz. A wraparound GPS antenna was used on the vehicle, which enabled continuous GPS coverage during the high spin rate of the powered flight phase. The Javad unit also produced estimates of the uncertainties in the position and velocity solution based on the number of satellites in view, shown in Figure 5(a), and the covariance of the onboard solution. The receiver estimates of position and velocity RMS errors are shown in Figure 5(b).

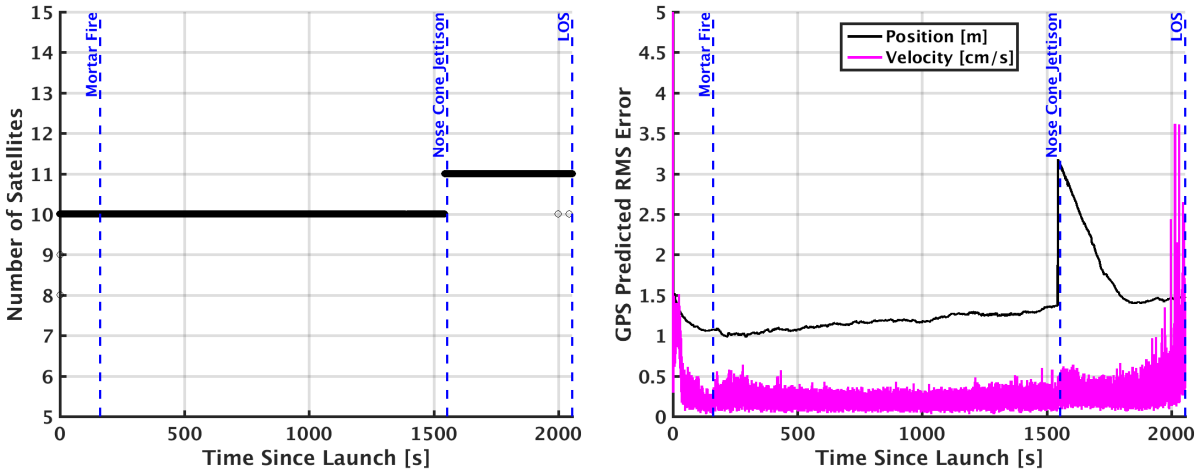

(a) Number of Satellites

(b) GPS Solution RMS Error

Figure 5: SR01 GPS Satellites and RMS Errors

C. Tracking Radar

Tracking of the sounding rocket and payload was provided via a C-band transponder and skin track from three primary radars, WFF Radars 3, 5, and 18. The radar data was provided at 50 Hz. The geometry of the radar stations relative to the as-flown trajectory is shown in Figure 6.

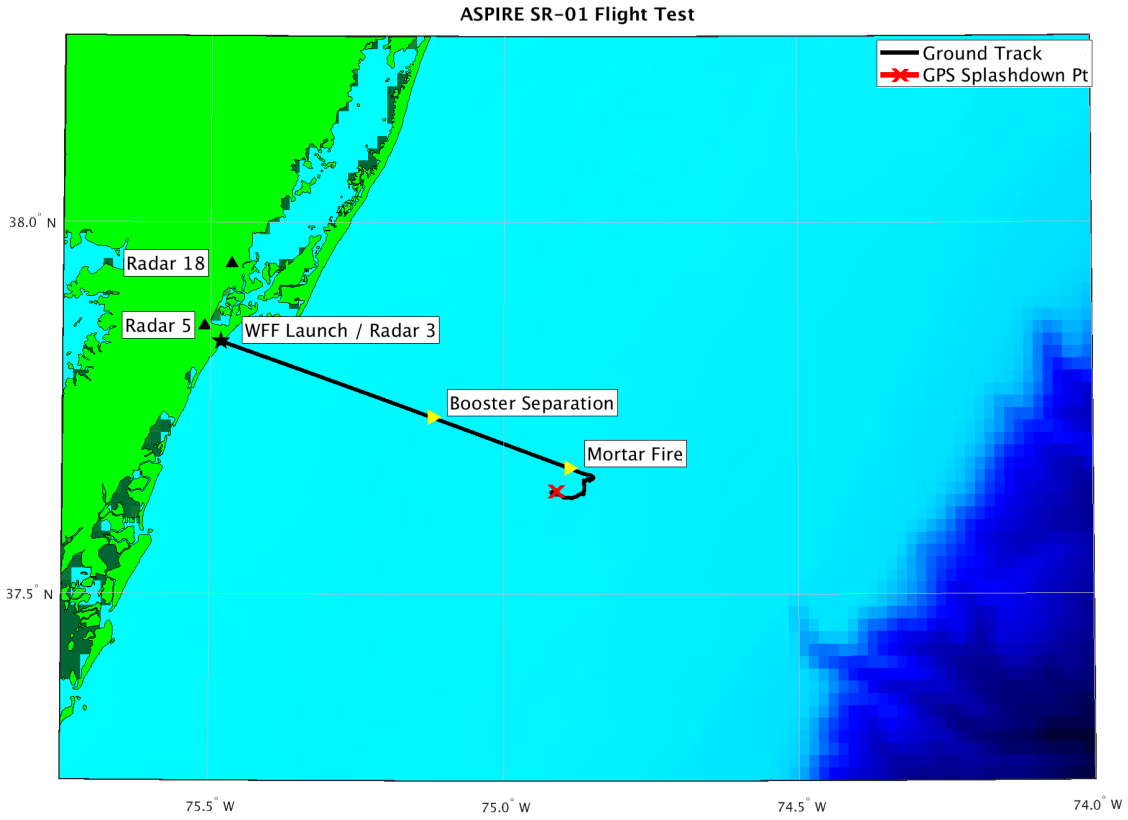

Figure 6: ASPIRE SR01 Ground Track and Radar Geometry

D. Meteorological Data

Knowledge of the atmospheric state at the time of testing was required in order to determine the conditions at parachute deployment (Mach number and dynamic pressure), examine the aerodynamic performance of the payload and parachute, and evaluate the performance of the triggering scheme. Specifically, vertical profiles of the atmospheric temperature, pressure, density, and winds spanning from the surface to an altitude of approximately 55 km were required. For SR01, these profiles were derived using a combination of measurements from radiosondes deployed on meteorological balloons and a meteorological analysis from the Goddard Earth Observing System Model, Version 5 (GEOS-5).

Table 1 describes the timeline of meteorological operations on the day of launch. Four meteorological balloons were launched between L-3 hours and L-1 hours, and reached altitudes between 35 km and 40 km. Because the balloons were not expected to reach altitudes above 40 km, the GEOS-5 profile for 12:00 UTC (8 AM local time) on the day of launch was used to estimate the atmospheric profiles above 40 km.

On the day of launch, four TA3000 meteorological balloons (Totex Corporation, Saitama, Japan) were released at regular intervals starting three hours before launch, as described in Table 1. The 3000 g latex balloons were filled with sufficient helium to provide 1800 g of free lift and released from ground altitude at Wallops Island. Figure 7(a) shows the first of the TA3000 balloons being carried out of the balloon operations building on Wallops Island for launch. The four balloons, designated by their launch times as L-3, L-2:15, L-1:45, and L-1 carried a single Lockheed Martin Sippican (Marion, MA) LMS-6 radiosonde each to peak altitudes of 35.3 km, 38.3 km, 39.9 km, and 37.9 km, respectively.

Figure 7(b) shows a schematic of the LMS-6 radiosonde. Each radiosonde contains a chip thermistor, an LMU6 capacitive humidity sensor, and a 12-channel differential GPS receiver. Measurements recorded on board the LMS-6 were telemetered to one of two ground stations on the WFF main base.

(a) TA3000 balloon being carried out of the balloon inflation building for launch

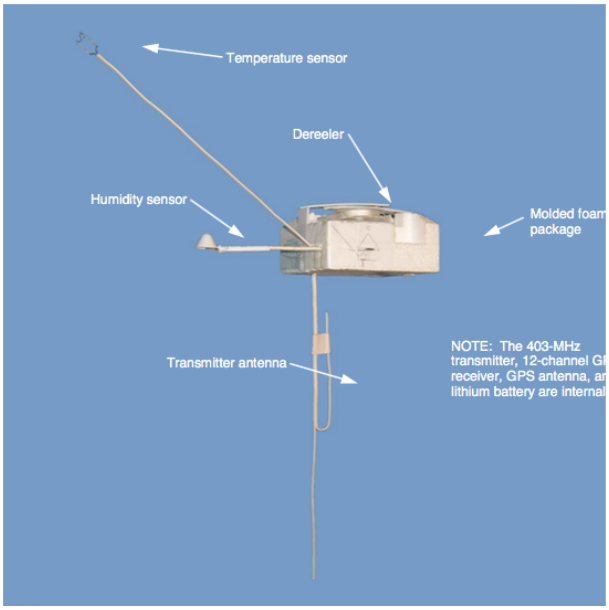

(b) Schematic of the LMS-6 radiosonde

Figure 7: Radiosonde Instrumentation

Table 1: SR01 atmospheric measurement timeline with significant events in **bold**

UTC Time	Local Time	Event
07:45	03:45	Met. balloon 1 launched
08:30	04:30	Met. balloon 2 launched
09:00	05:00	Met. balloon 3 launched
09:27	05:27	Met. balloon 1 burst
09:45	05:45	Met. balloon 4 launched
10:20	06:20	Met. balloon 2 burst
10:45	06:45	**SR01 launch**
10:48	06:48	**Mortar fire**
10:52	06:52	Met. balloon 3 burst
11:11	07:11	**Nosecone separation**
11:20	07:30	**Payload splashdown**
11:34	07:34	Met. balloon 4 burst
12:00	08:00	Nominal time for GEOS-5 12:00 analysis

III. Reconstruction Methods

The instrumentation utilized during the ASPIRE SR01 mission provided an extensive set of measurement data from which reconstruction was performed. The following section describes the methodologies used to reconstruct the trajectory and atmosphere given the measurements taken during flight.

A. Atmosphere Reconstruction

1. Weather Balloon Measurements

Temperature, humidity, and altitude were measured directly by the on-board instrumentation, and the atmospheric winds are derived from the GPS velocity measurements. The atmospheric pressure was derived from the temperature and altitude measurements by assuming that the atmosphere was in hydrostatic equilibrium:

$$\frac{dP}{P} = \frac{-g}{R}\frac{dZ}{T_v} \tag{1}$$

where P is the atmospheric pressure, T_v is the virtual temperature of the moist air, Z is the geopotential height, R=287.058 J kg^{-1} K^{-1} is the specific gas constant for dry air, and $g = 9.81$ m/s^2 is the acceleration of gravity at the Earth's surface. The virtual temperature of moist air is the temperature at which a parcel of dry air would have a pressure and density equivalent to that of the moist air. It is given by:

$$T_v = \frac{T}{1 - \frac{e}{P}(1-\epsilon)} \tag{2}$$

where e is the vapor pressure, and the ratio of the molar masses of vapor and dry air was assumed to be $\epsilon = 0.622$[8]. The geopotential height (Z) was derived from the geodetic altitude and latitude using the 1984 World Geodetic System (WGS84) model.

Table 2 lists the uncertainties associated with the radiosonde measurements, at the 3σ level. Where the uncertainties were not stated by the manufacturer [9], the values for radiosondes of the same class from the 2014 World Meteorological Organization (WMO) report on atmospheric measurement techniques [10] were used. Figure 8 shows the temperature, density, and wind measurements recorded by the four radiosondes. The wind measurements have been low-pass filtered with a cut-off frequency of 1/600 Hz, to yield a wavelength of approximately 1 km in the vertical direction.

Table 2: LMS-6 measurement 3σ uncertainties

Measurement	Uncertainty	Notes
Temperature	0.45 K	[9]
Humidity	7.5%RH	Valid to $P = 20$ hPa[9]
Wind Velocity	1.65 m/s	Vector magnitude [10]
Pressure ($P > 100$ hPa)	1.8 hPa	[10]
Pressure (10 hPa $< P <$ 100 hPa)	0.6 hPa	[10]
Pressure ($P < 10$ hPa)	0.075 hPa	[10]

2. Atmospheric Model

Since the TA3000 balloons have a burst altitude of approximately 40 km, no in-situ measurements were available above this altitude. Therefore, the atmospheric profile above 40 km was obtained from a GEOS-5 analysis. GEOS-5 is a group of interconnected predictive models for the Earth system (atmosphere, land, and ocean) developed by the Global Modeling and Assimilation Office (GMAO) at Goddard Space Flight Center (GSFC) [11]. GEOS-5 assimilates measurements from a variety of sources including daily radiosonde launches by the National Weather Service (NWS), ground station measurements, satellite measurements, radar wind measurements, and surface ship and buoy observations to generate regular global forecasts and analyses of the current atmospheric state.

The GEOS-5 analysis of the atmospheric state is calculated daily at three hour intervals, starting at 0:00 UTC. The analyses are produced on a grid with a horizontal resolution of 0.5 deg in latitude and 0.625 deg in longitude.

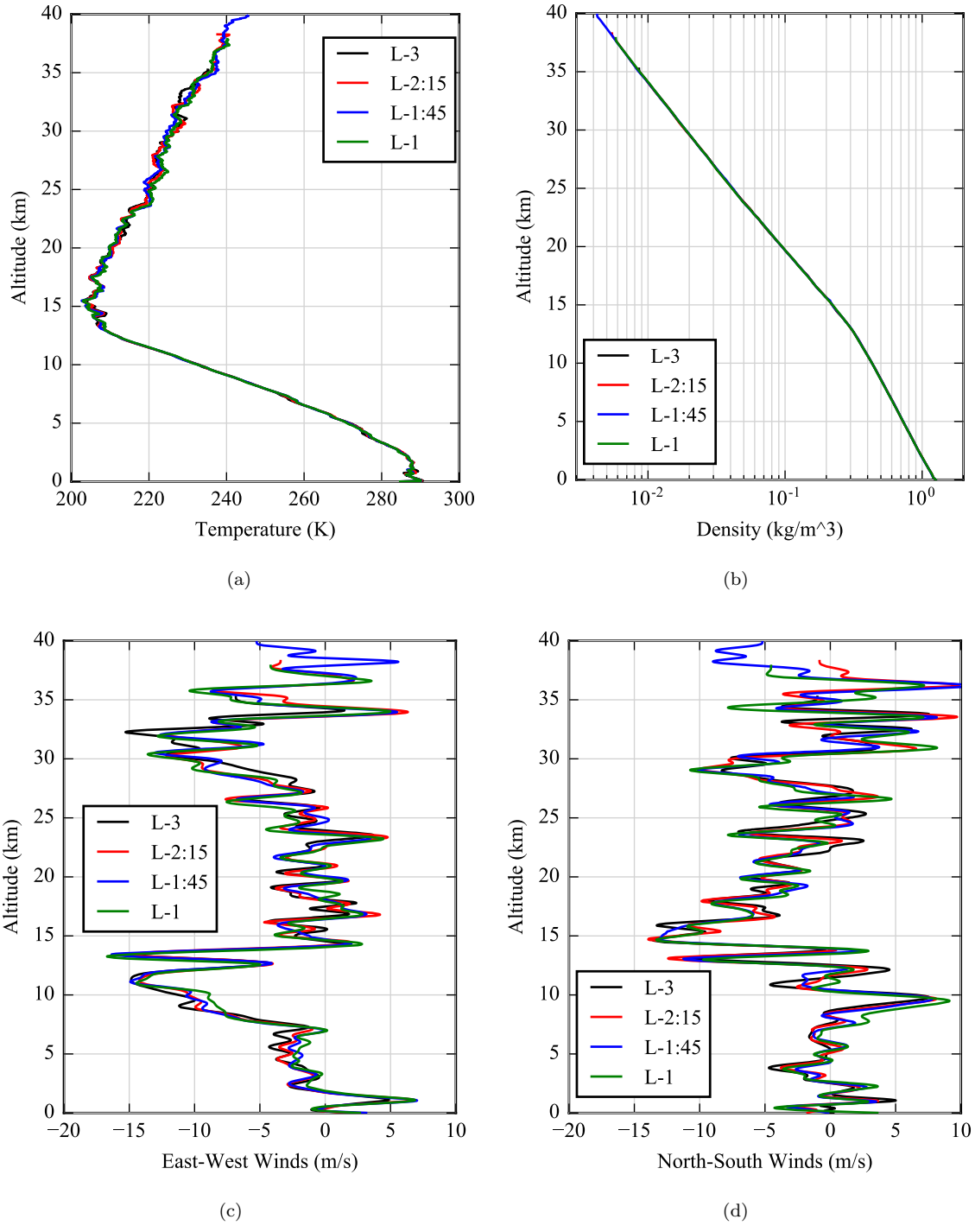

Figure 8: Radiosonde Measurements

Vertical profiles are output at 42 pressure levels ranging from 1000 hPa near the surface to 0.1 hPa (approximately 65 km above sea level) [12]. For SR01, the GEOS-5 analysis for 12:00 UTC (8 am local time) was used to obtain vertical profiles for the atmospheric temperature, pressure, density, and winds at the grid location closest to Wallops Island: (37.75 deg, -75.0 deg).

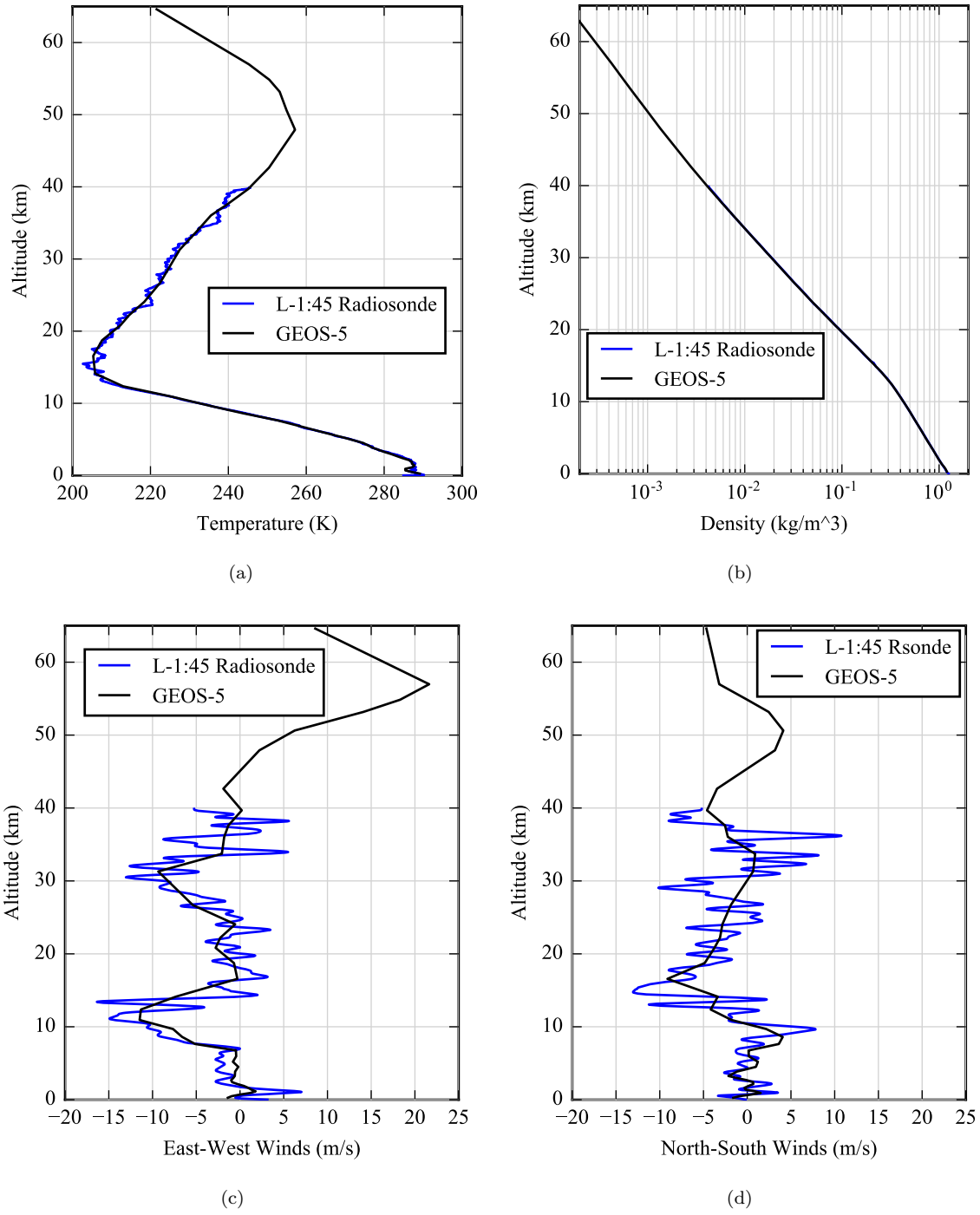

Figure 9: GEOS-5 analysis for 12:00 UTC on the day of launch. The measurements from the L-1:45 radiosondes, which reached the highest altitude, are shown in blue for comparison.

Figure 9 shows the vertical profiles of temperature, density, and winds for the 12:00 UTC GEOS-5 analysis. Below 39.9 km, the GEOS-5 results are compared against the measurements from the L-1:45 radiosonde, which reached the highest altitude. In general, the GEOS-5 profile captures the mean of the radiosonde measurements. However, the radiosonde measurements exhibit small-scale variations that are not captured by GEOS-5. The variations in the

winds can be quite large, leading to differences between the GEOS-5 profile and measurements in excess of 10 m/s. The differences between the radiosonde temperature measurements and the GEOS-5 profile are significantly smaller (less than 4 K), and the GEOS-5 temperature profile does not show a bias relative to the measurements. Because the radiosonde pressure and density measurements are integral functions of temperature and the measured temperature follows the GEOS-5 profiles quite closely, the radiosonde pressure and density measurements are also in very close agreement with the GEOS-5 profile.

B. Trajectory Reconstruction

The ASPIRE SR01 trajectory reconstruction was performed using a Matlab-based Iterative Extended Kalman Filter (IEKF) code known as NewSTEP[13, 14, 15, 16]. This software is a generalization of the Statistical Trajectory Estimation Program (STEP)[17, 18] that was developed by NASA Langley Research Center and applied to launch and entry vehicle trajectory reconstruction analyses during the 1960s-1980s. The NewSTEP code borrows largely from STEP, but includes various enhancements to the core code that have been developed to accommodate the reconstruction needs of recent flight projects.

NewSTEP was configured to process data from the GLN-MAC gimballed IMU measurements using a process developed for the Low Density Supersonic Decelerator project (LDSD)[19, 20, 21]. Many past applications of gimbaled IMU reconstructions have made use of an equivalent strapdown representation of the linear accelerations and angular rates in the estimation filter by transforming the platform data into a strapdown frame via the measured gimbal angle[22, 23]. This approach has the advantage of producing a strapdown representation of the inertial measurements without any error buildup due to roll gyro scale factor. The drawback to this method is that resolver angular rate and acceleration uncertainty will degrade the measurements substantially due to resolver angle quantization, amplified by errors from numerical differentiation.

For the LDSD flight reconstructions, an alternate approach was devised in which the trajectory of the LN-200 itself was reconstructed from the measurement data using the Kalman filter approach to blend IMU measurements with GPS and Radar. The output of this process is a kinematic reconstructed trajectory of the LN-200 in an IMU-relative frame through inertial space. After reconstructing the LN-200 trajectory, the resolver angle profile was used to transform the state outputs into the vehicle aerodynamic coordinate frame. Additionally, the reconstructed mass properties were incorporated in order to translate the reconstructed state of the vehicle to the center of gravity (CG). The vehicle mass properties used for the reconstruction were computed using pre-flight mass models that were adjusted to match the as-flown timeline.

At this point in the process, the resolver quantization uncertainty corrupts the reconstructed vehicle state, but this uncertainty is an algebraic mapping at each instant in time such that the resolver angle uncertainties do not propagate over time. After transforming the LN-200 state to the vehicle body frame at the CG, the freestream atmosphere was computed as a function of altitude from a table lookup, and the atmospheric relative state (angle of attack, Mach number, dynamic pressure, etc.) was computed. The same overall process developed for the LDSD project was adopted for the ASPIRE project.

IV. Flight Data Analysis

A. Reconstructed Atmosphere

Figure 10 shows the reconstructed atmospheric profile for the morning of October 4, 2017. The solid black lines denote the mean values, while the dashed black lines indicate the corresponding 3σ bounds. The mean monthly profiles for the month of October from the 1983 Range Reference Atmosphere (RRA) for Wallops Island [24] are also shown for reference. For ease of comparison, Figure 10(b) shows the percent difference between the reconstructed density and the mean monthly profile. The local atmospheric profile was atypical for the season in two key ways. First, the East-West winds were significantly lower than expected on the day of launch, especially below 15 km and above 30 km. Secondly, the atmospheric density was higher than expected in the 5 km to 25 km range. These differences were captured by both the GEOS-5 analysis and the radiosonde measurements.

Below 40 km, the nominal profiles in Figure 10 correspond to the measurements recorded by the L-1:45 radiosonde, which reached a peak altitude of 39.9 km seven minutes after the experiment was launched. The 3σ bounds include the measurement uncertainties listed in Table 2, as well as estimates for the temporal and spatial variations in the atmosphere. At each altitude, the maximum difference among the radiosonde measurements was used to estimate the small-scale temporal and spatial variations in the measurements. Above 38 km, where fewer than three overlapping radiosonde measurements are available, the maximum observed difference between the four radiosondes in the 0 km to 38 km range was used. Note that the maximum *absolute* difference was used for the temperature and winds, while

the maximum *percentage* difference was used for the pressure and density, which decrease exponentially with altitude. The total uncertainty in each quantity was calculated as the root-sum-square of the measurement uncertainties and the estimated spatial and temporal variations.

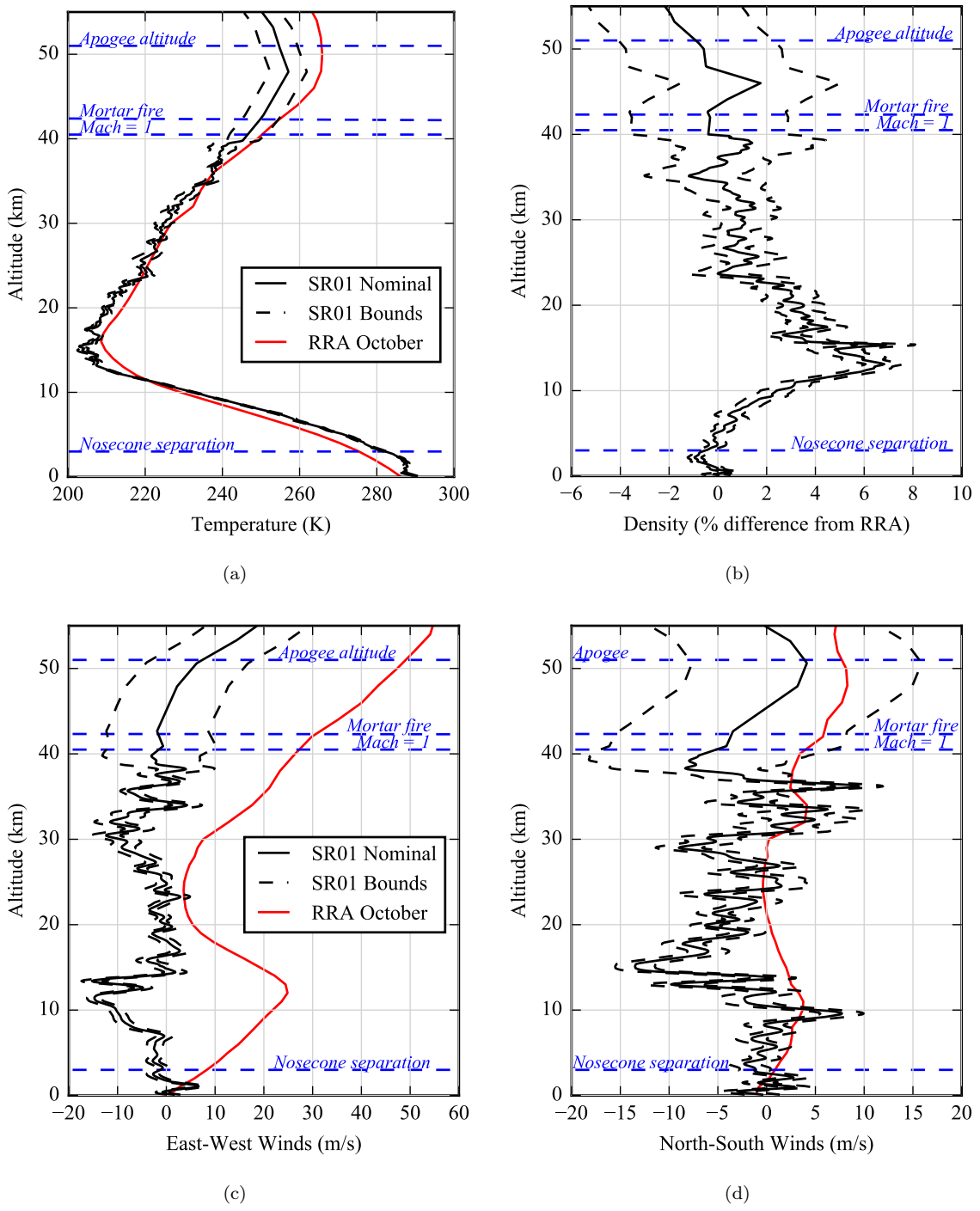

Figure 10: SR01 reconstructed atmosphere. The mean monthly values from the 1983 RRA are shown in red for reference. The altitudes at which key events occur are highlighted in blue.

Above 40 km, the nominal reconstructed atmosphere corresponds to the GEOS-5 profile. Since no in-situ measurements are available at these altitudes, and since the GEOS-5 profile does not capture the small-scale variations in the atmosphere (Figure 9), the uncertainties in the atmospheric profile are larger above 40 km. At these altitudes, the uncertainties were assumed to be equal to the largest observed differences between the radiosondes and the GEOS-5 profile in the 0 km to 38 km range.

The altitudes at which key events in the flight sequence occurred are denoted in Figure 10 by dashed blue lines. Note that at the parachute deployment (mortar fire) altitude, the uncertainty in temperature was ±4.7 K, the uncertainty in pressure was 6.2 Pa, the uncertainty in density was 3.2% of the freestream, and the uncertainty in the total wind velocity was less than 16 m/s.

B. Reconstructed Trajectory

The test vehicle trajectory was reconstructed from the LN-200 accelerations and angular rates, GPS, and radar measurements following the process described previously. The reconstruction was initialized at launch, using initial conditions from the on-board navigation solution. Reconstruction of state variables was performed until loss of signal at 2056.19 s, just prior to vehicle splashdown in the Atlantic ocean.

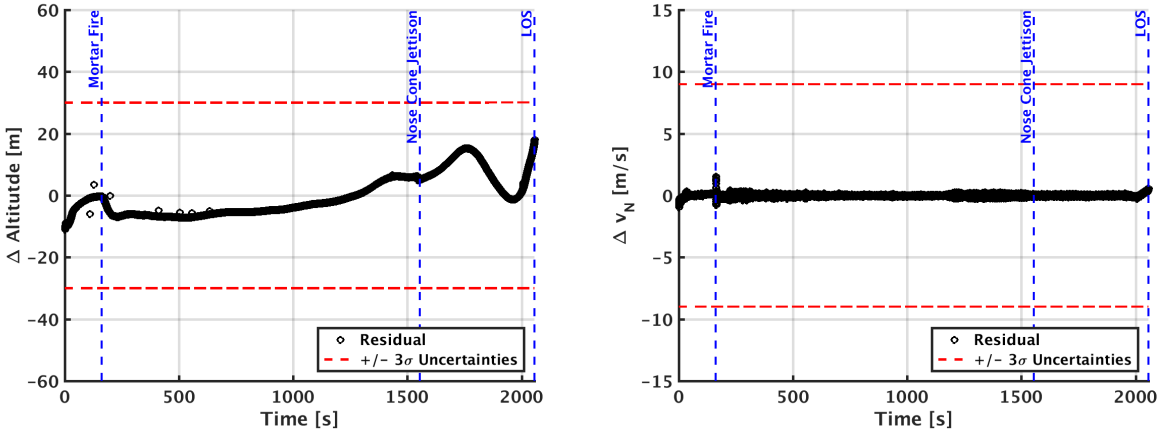

(a) Geodetic Altitude Residuals

(b) North Velocity Residuals

Figure 11: ASPIRE SR01 GPS Measurement IEKF Residuals

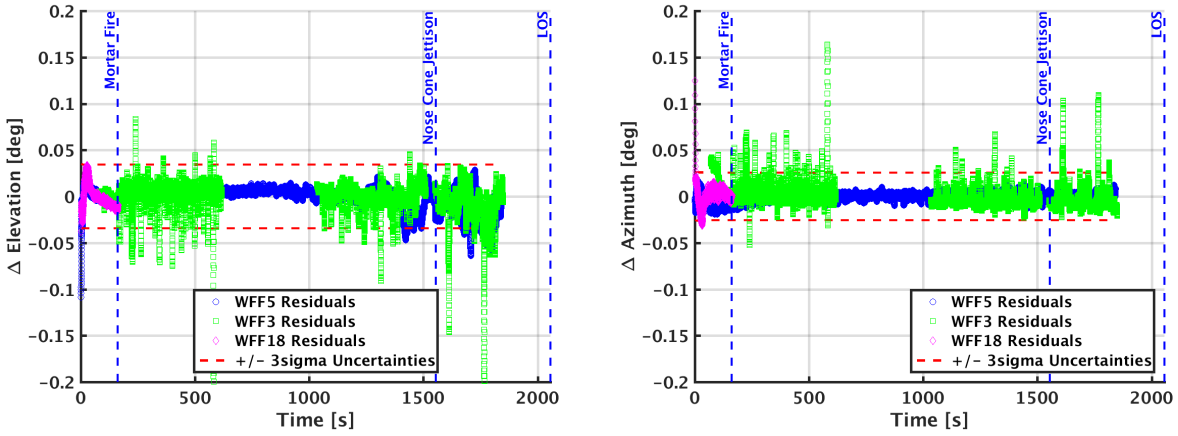

(a) Radar Elevation Residuals

(b) Radar Azimuth Residuals

Figure 12: ASPIRE SR01 Radar Measurement IEKF Residuals

The GPS measurement residuals are shown in Figure 11. The residuals are computed by taking the difference between the measurement observed during flight and the predicted measurement generated by the filter. An inspection of the measurement residuals provides an assessment of the filter performance relative to the measurement uncertainties. It is evident that the residual values largely fall inside of the 3σ uncertainties, which is an indicator of good filter performance. While not shown, the residual results for geodetic latitude, longitude, east velocity and down velocity are comparable to those shown in Figure 11. The radar data required some editing due to dropouts. Radar WFF3 exhibited several dropouts or loss of transponder lock over the trajectory that made the data unusable. Data from 0-70 s, 619-1033 s, 1451-1460, 1511-1550 were edited out and not utilized for reconstruction. WFF5 maintained

a good lock on the transponder over the entire trajectory. WFF18 tracked the vehicle until a time of 164 s (just after peak parachute load) into the trajectory, where it lost transponder lock and reverted into a skin track mode. The skin track data exhibited more noise than transponder data and thus were not included in the reconstruction. All data with elevation angles of less than 1 deg were removed from the filter inputs because of increased noise due to refraction errors. The radar residuals processed in the filter are indicative of good filter performance, as shown in Figure 12.

Details of the reconstructed trajectory are shown in the following figures. Figure 13 shows the reconstructed altitude and Mach number time histories from launch until 200 seconds, by which time the payload has reached low subsonic flight conditions. Figure 14 shows the dynamic pressure time history. The sensed accelerations at the vehicle center of mass are shown in Figure 15, and the vehicle angular velocity components are shown in Figure 16. Finally, vehicle attitude and trajectory angles are shown in Figure 17.

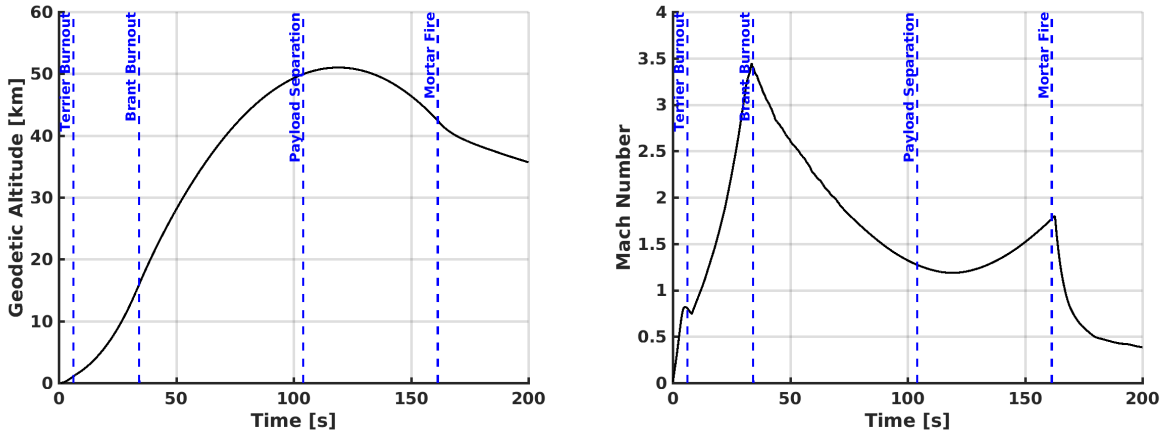

(a) Altitude (b) Mach Number

Figure 13: ASPIRE SR01 Trajectory: Altitude and Mach Number

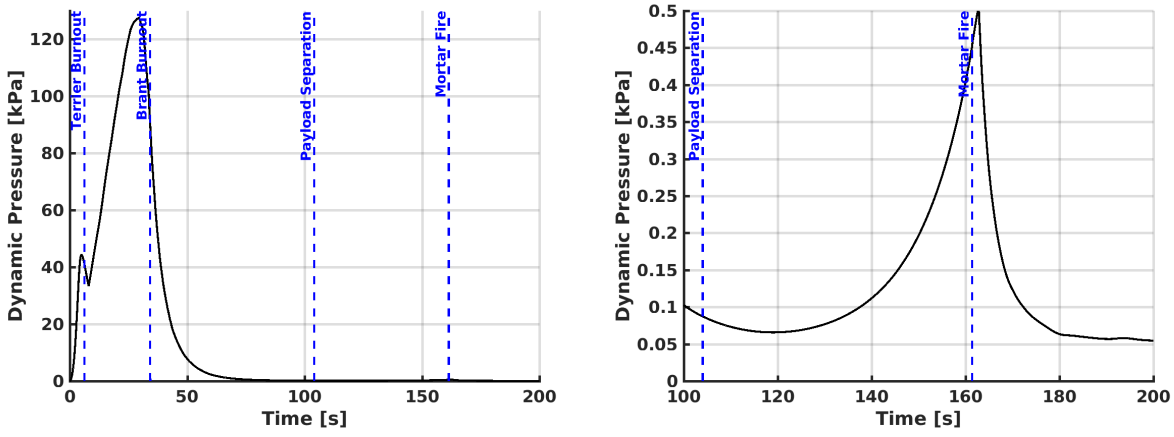

(a) Dynamic Pressure (b) Dynamic Pressure (detail)

Figure 14: ASPIRE SR01 Trajectory: Dynamic Pressure

On ascent the Brant stage reached a peak Mach number of 3.4 at the time of burnout, and a maximum spin rate of just over 1200 deg/s. After burnout, the vehicle coasted and then despun to a residual spin rate of 30 deg/s before the payload separation occurred at an altitude of just under 50 km. The NIACS thrusters were then used to null out the residual spin rate and to orient the pitch and yaw axes of vehicle for near zero total angle of attack at mortar fire. The payload reached an apogee of approximately 51 km after separation from the Brant stage, at a Mach number of 1.27.

The parachute mortar fire occurred at an altitude of approximately 42.4 km, with corresponding Mach number

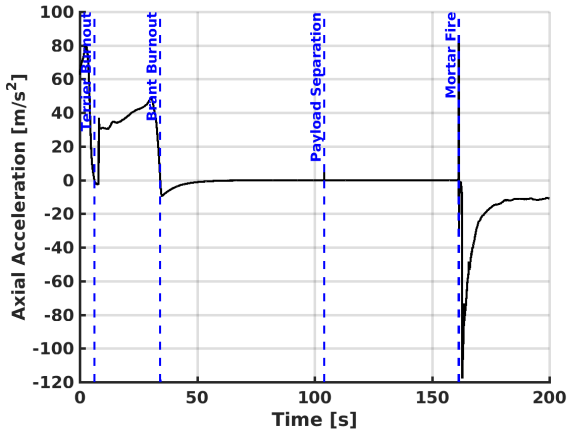

(a) Axial Acceleration

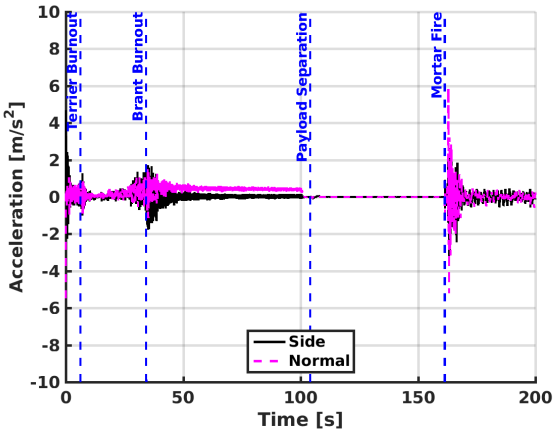

(b) Side and Normal Acceleration

Figure 15: ASPIRE SR01 Trajectory: Acceleration

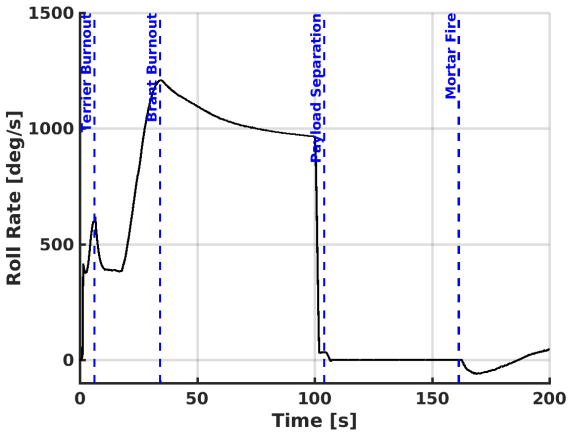

(a) Roll Rate

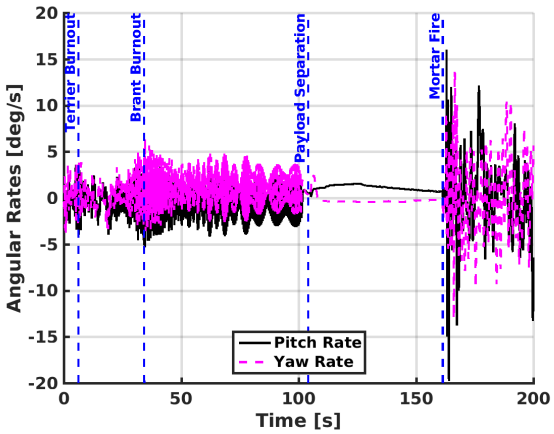

(b) Pitch and Yaw Rates

Figure 16: ASPIRE SR01 Trajectory: Angular Rates

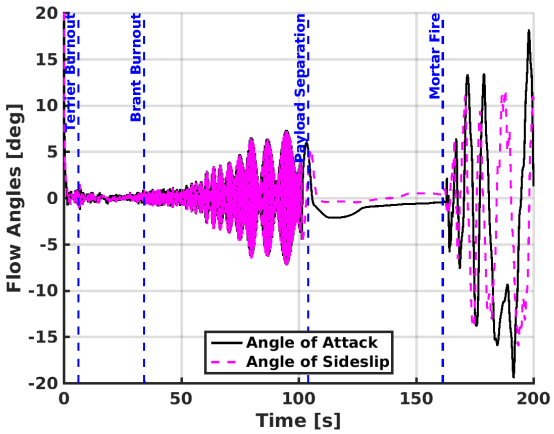

(a) Flow Angles

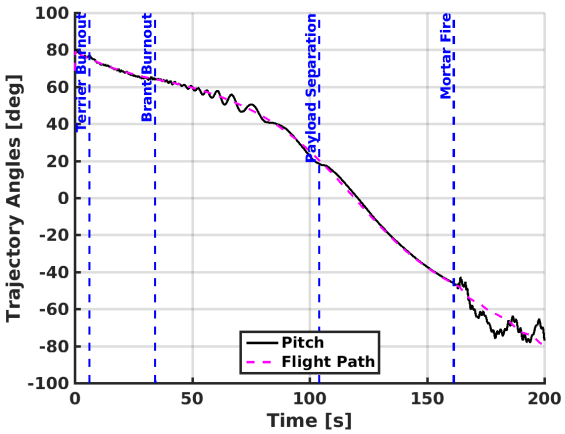

(b) Trajectory Angles

Figure 17: ASPIRE SR01 Trajectory: Attitude Angles

of 1.77 and dynamic pressure of 452.53 Pa. After mortar fire, the parachute inflated successfully. The peak load condition was reached at a Mach number of 1.77 and dynamic pressure of 494.88 Pa. Recall that the target condition was a Mach number of approximately 1.7 and a dynamic pressure of 474 Pa. After parachute inflation, the vehicle decelerated rapidly, crossing the Mach 1 boundary at a time of approximately 167 s from launch. After reaching terminal velocity, the payload descended to land in the Atlantic ocean. The nose cone containing ballast was jettisoned at an altitude of approximately 3 km. The last data point just prior to landing in the ocean occurred at a time of 2056.19 s after launch and an altitude of approximately 25 m (geodetic). After landing in the water, the payload and parachute were recovered and brought back to shore for inspection and recovery of onboard recorded data.

C. Test Conditions

A summary of the conditions at important events in the trajectory is provided in Table 3.

Table 3: Trajectory conditions at key test events

Event	**Time from Launch**	**Mach**	**Dynamic Pressure**	**Wind-Relative Velocity**	**Geodetic Altitude**	**Flight Path Angle**
	sec		*Pa*	*m/s*	*km*	*deg*
Launch	0.00	0.01	8.07	3.61	-0.02	36.2
Spin Up	1.18	0.21	3070.38	70.52	0.02	79.8
Terrier Burnout	6.23	0.80	41108.93	273.26	1.06	76.3
Brant Ignition	8.02	0.74	33481.89	253.30	1.52	74.7
Mach 1	11.98	1.00	52824.66	338.08	2.64	71.7
Mach 2	23.16	2.00	112192.78	637.46	7.64	67.1
Mach 3	30.04	3.00	126143.61	876.17	12.37	64.9
Brant Burnout	34.27	3.40	89587.04	979.30	15.97	64.1
Despin Begin	100.09	1.32	102.08	423.54	49.27	25.4
Payload Separation	104.03	1.27	87.15	407.80	49.92	20.6
Apogee	119.04	1.19	65.74	379.66	51.00	0.0
Mortar Fire	161.41	1.77	452.53	560.29	42.40	-46.4
Line Stretch	162.37	1.79	491.82	567.74	42.01	-47.1
Peak Load	162.88	1.77	494.88	560.94	41.80	-47.4
Mach 1.4	164.34	1.40	334.20	443.43	41.26	-48.9
Mach 1.0	166.99	1.00	188.93	315.52	40.49	-52.9
Mach 0.5	179.61	0.50	64.34	154.96	38.25	-64.5
Nose Cone Jettison	1554.09	0.03	45.01	10.06	3.027	-85.2
Loss of Signal	2056.19	0.02	38.00	7.85	0.02	-41.2

V. Conclusions

The Advanced Supersonic Parachute Inflation Research Experiment project flew its first sounding rocket flight test on October 4th, 2017. This first flight was used to validate the test architecture, including demonstrating powered flight and successful triggering of events. The flight test successfully accomplished these objectives, and also provided measurements of decelerator technology performance. The sensor measurements acquired during the flight test were of good quality, allowing a vehicle trajectory, atmosphere, and aerodynamic reconstruction to be performed using a Kalman filter approach to blend all available data. The same overall process will be utilized for future flight tests.

References

[1] O'Farrell, C., Clark, I., and Adler, M., "Overview of the ASPIRE Project," 14th International Planetary Probe Workshop, The Hague, NL, June 2017.

[2] Tanner, C., Clark, I., and Chen, I., "Overview of the Mars 2020 Parachute Risk Reduction Plan," IEEE Aerospace Conference, March 2018.

[3] Clark, I. and Tanner, C., "A Historical Summary of the Design, Development, and Analysis of the Disk-Gap-Band Parachute," IEEE Aerospace Conference, March 2018.

[4] Cruz, J., Way, D., Shidner, J., Davis, J., Adams, D., and Kipp, D., "Reconstruction of the Mars Science Laboratory Parachute Performance," *Journal of Spacecraft and Rockets*, Vol. 51, No. 4, 2014, pp. 1185-1196.

[5] O'Farrell, C., Karlgaard, C., Tynis, J., and Clark, I., "Overview and Reconstruction of the ASPIRE Project's SR01 Supersonic Parachute Test," IEEE Aerospace Conference, March 2018.

[6] Dutta, S., Queen, E., Bowes, A., and Ivanov, M., "ASPIRE Flight Mechanics Modeling and Post Flight Analysis," AIAA Paper, June 2018.

[7] Anon., "NASA Sounding Rocket Program Handbook," Sounding Rockets Program Office, Suborbital and Special Orbital Projects Directorate, Goddard Space Flight Center, Wallops Flight Facility, Wallops Island, Virginia, 810-HB-SRP, June 2005.

[8] Moran, M. J. and Shapiro, H. N., *Fundamentals of Engineering Thermodynamics*, J. Wiley and Sons, 5th Edition, 2004.

[9] Anon., "LMS6 Radiosonde Operator's Manual," Lockheed Martin Sippican, 2013.

[10] Anon., "Guide to Meteorological Instruments and Methods of Observation," World Meteorological Organization, 2014.

[11] Rienecker, M. M., Suarez, M. J., Todling, R., Bacmeister, J., Takacs, L., Liu, H.-C., Gu, W., Sienkiewicz, M., Koster, R., Gelaro, R., Stajner, I., and Nielsen, J., "The GEOS-5 Data Assimilation System - Documentation of Versions 5.0.1, 5.1.0, and 5.2.0," NASA TM-2008-104606, 2008.

[12] Bosilovich, M., Lucchesi, R., Suarezn, M., "MERRA-2: File Specification," GMAO Interoffice Note, September 2016.

[13] Karlgaard, C. D., Tartabini, P. V., Blanchard, R. C., Kirsch, M., and Toniolo, M. D., "Hyper–X Post–Flight Trajectory Reconstruction," *Journal of Spacecraft and Rockets*, Vol. 43, No. 1, 2006, pp. 105–115.

[14] Karlgaard, C. D., Tartabini, P. V., Martin, J. G., Blanchard, R. C., Kirsch, M., Toniolo, M. D., and Thornblom, M. N., "Statistical Estimation Methods for Trajectory Reconstruction: Application to Hyper-X," NASA TM-2009-215792, August 2009.

[15] Karlgaard, C. D., Beck, R. E., Derry, S. D., Brandon, J. M., Starr, B. R., Tartabini, P. V., and Olds, A. D., "Ares I-X Trajectory Reconstruction: Methodology and Results," *Journal of Spacecraft and Rockets*, Vol. 50, No. 3, 2013, pp. 641–661.

[16] Karlgaard, C. D., Kutty, P., Schoenenberger, M., Munk, M. M., Little, A., Kuhl, C. A., and Shidner, J., "Mars Science Laboratory Entry Atmospheric Data System Trajectory and Atmosphere Reconstruction," *Journal of Spacecraft and Rockets*, Vol. 51, No. 4, 2014, pp. 1029–1047.

[17] Wagner, W. E., "Re-Entry Filtering, Prediction, and Smoothing," *Journal of Spacecraft and Rockets*, Vol. 3, No. 9, 1966, pp. 1321–1327.

[18] Wagner, W. E. and Serold, A. C., "Formulation on Statistical Trajectory Estimation Programs," NASA CR-1482, January 1970.

[19] Kutty, P., Karlgaard, C. D., Blood, E., O'Farrell, C., Ginn, J., Schoenenberger, M., and Dutta, S., "Supersonic Flight Dynamics Test: Trajectory, Atmosphere, and Aerodynamics Reconstruction," American Astronautical Society, AAS Paper 15-224, January 2015.

[20] Blood, E., Ivanov, M., O'Farrell, C., Ginn, J., Kutty, P., Karlgaard, C., and Dutta, S., "LDSD Supersonic Flight Dynamics Test 1: Post-flight Reconstruction," IEEE Aerospace Conference, Paper 2621, March 2015.

[21] Karlgaard, C. D., O'Farrell, C., Ginn, J., and Van Norman, J., "Supersonic Flight Dynamics Test 2: Trajectory, Atmosphere, and Aerodynamics Reconstruction," American Astronautical Society, AAS Paper 16-217, February 2016.

[22] Olds, A. D., Beck, R. E., Bose, D. M., White, J. P., Edquist, K. T., Hollis, B. R., Lindell, M. C., Cheatwood, F. M., Gsell, V. T., and Bowden, E. L., "IRVE-3 Post-Flight Reconstruction," AIAA Paper 2013-1390, March 2013.

[23] Heck, M. L., Findlay, J. T., Kelly, G. M., and Compton, H. R., "Adaptation of a Strapdown Formulation for Processing Inertial Platform Data," *Journal of Guidance, Control, and Dynamics*, Vol. 7, No. 1, 1984, pp. 15–19.

[24] Anon., "Range Reference Atmosphere, 0-70 km Altitude, Wallops Island, Virginia," Meteorology Group, Range Commanders Council, Report Number 364-83, 1983.